



Cite this: *RSC Adv.*, 2017, 7, 30295

Received 17th January 2017  
Accepted 6th June 2017

DOI: 10.1039/c7ra00706j

rsc.li/rsc-advances

# Grain size reduction on nanostructured TiO<sub>2</sub> thin films due to annealing

Zaki S. Khalifa 

TiO<sub>2</sub> thin films have been deposited at 300 °C on quartz substrates by a metal–organic chemical vapor deposition technique. The obtained films have been annealed at different temperatures up to 1100 °C. X-ray diffraction studies show that the obtained films maintain the anatase phase till 800 °C annealing temperature, and the rutile phase appears at 900 °C. Extra unidentified peaks appear at 1000 °C, and 1100 °C. Raman microscopy has been used to identify the obtained films. The obtained spectra show the normal modes of vibrations of the pure and mixed phases. Scanning electron microscopy graphs show grain size shrinkage concurrent to the appearance of the rutile phase. A slight band gap reduction has been calculated from UV-Vis transmittance spectrophotometry measurements. DC conductivity curves show three regions with different activation energies.

## 1. Introduction

TiO<sub>2</sub> thin films have been involved in many applications such as electrochromism,<sup>1</sup> lithium batteries,<sup>2</sup> photocatalysis,<sup>3</sup> H<sub>2</sub> production,<sup>4</sup> dye sensitized solar cells,<sup>5</sup> and gas sensing.<sup>6</sup> The optical and electrical properties of the TiO<sub>2</sub> thin films depend on the structure and morphology of the deposited material which is dictated beside the preparation method by the preparation conditions, and/or post deposition treatments. Moreover, specific applications rely on the crystalline structure and morphology of the active material. For example, the anatase phase shows better electrochemical properties than rutile,<sup>7</sup> while the mixed phase shows better photon to electron conversion properties than both single phases.<sup>8</sup> Raising the deposition temperature causes structural and morphological changes in the TiO<sub>2</sub> nanoparticles. They include amorphous to crystalline, and phase to phase transformations.<sup>9</sup>

TiO<sub>2</sub> has three famous polymorphs, anatase, brookite, and rutile. They consist of octahedra shared by edges and corners. Octahedron has 12 edges. In anatase 4 of these edges are shared with neighboring octahedra, but in rutile only 2 are. At the same time, the anatase octahedron is corner shared with 8 octahedra, while rutile is shared by 4. Anatase has 4 polyhedra per unit cell, and rutile has 2. All these structure differences have their impact on the electronic structure which can be investigated by optical and electrical measurements. Phase transformation among the above mentioned TiO<sub>2</sub> three polymorphs has been studied before.<sup>9,10</sup> In fact, if we need a better understanding of phase transformations we have to think about Gibb's free energy function. In other words, thermodynamics will enable us

to collect the affecting parameters in phase transformation in one equation. Change in Gibb's free energy for bulk is the difference between the standard free energy of formation of the individual phases.<sup>11,12</sup> In the nanoscale additional terms should be added so:<sup>13</sup>

$$\Delta G_{A-R} = (\Delta G_{V,R}(T) - \Delta G_{V,A}(T)) + (\gamma_R A_R - \gamma_A A_A) + (\Delta P_R V_R - \Delta P_A V_A) \quad (1)$$

where subscripts A, and R stands for anatase, and rutile phases.  $\Delta G_{A-R}$ , is the Gibb's free energy of transformation from anatase to rutile,  $\Delta G_V$  is the volume free energy,  $\gamma$  is the surface free energy,  $\Delta P$  is a surface stress related pressure,  $A$  is the surface area, and  $V$  is the molar volume. For phase transformation to take place,  $\Delta G_{A-R}$  should be negative. If  $\Delta G_{A-R} = 0$ , nanocrystalline anatase exists in equilibrium with rutile at a specific temperature, and crystal size. Bulk rutile is more stable than bulk anatase at ambient conditions, and higher temperatures.<sup>14,15</sup> This fact has been confirmed by experiment.<sup>16</sup> However, this order is reversed in the nanoscale. Theoretically, Oliver *et al.*<sup>17</sup> and, Lazzeri *et al.*<sup>18,19</sup> showed that the average surface energy of the anatase phase surfaces has a lower value compared to that of the rutile. Wulff's construction based on Lazzeri *et al.* calculations agrees with the anatase macrocrystal existing in nature.<sup>20</sup> Kinetic studies conducted on TiO<sub>2</sub> powder by sol-gel confirmed anatase phase stability compared to rutile at small particle sizes due to the mentioned surface energy differences.<sup>21</sup> Thermodynamic analysis considering the volume free energy, surface free energy, and surface stress revealed that the particle size at the phase stability crossover is 14 to 15 nm,<sup>22</sup> which confirms Gribb, and Banfield results.<sup>21</sup> For thin films crystallite, and grain sizes are bigger.<sup>10,23</sup>

The driving force for this transformation usually is the increase of annealing temperature<sup>12,21</sup> but combination of

Department of Physics, Beni-Suef University, Beni-Suef 62111, Egypt. E-mail: zaki.khalifa@science.bsu.edu.eg; Fax: +20822334551; Tel: +201004829670



pressure and temperature also control this transformation for deposition processes.<sup>9,10,24</sup> Moreover, super-saturation can be achieved by controlling the precursor solution environment. In other words, chemical potential, and the number of moles, or equivalently the chemical activities of the reactants, and products can play a significant role in the phase, and shape of the deposited TiO<sub>2</sub> films. Roy *et al.*<sup>25</sup> have studied not only the deposition conditions but also the properties of TiO<sub>2</sub> thin films produced by solution bath deposition method. This can be translated as another term in eqn (1).

This study aims to explore the effect of annealing temperature on the structure, morphology, optical, and electrical properties of TiO<sub>2</sub> thin films prepared by MOCVD.

## 2. Material and methods

### 2.1. Preparation of the films

Thin films of TiO<sub>2</sub> have been deposited on quartz substrates by a hot wall chemical vapor deposition technique at temperature 300 °C. 25 × 12 × 1 mm quartz substrates have been used. Before loading, the substrates have been washed by detergent, distilled water, acetone, and isopropyl alcohol. The reactor consists of a stainless steel tube attached from one side to a pressure gauge, and a mechanical pump, and from the other side to oxygen, and precursor inlets. It has been put in a horizontal furnace. The precursor is titanium tetra isopropoxide, TTIP 97 +% pure, Alfa Aesar, USA. A 0 Torr pressure has been maintained in the reactor during heating. After that O<sub>2</sub> has been introduced to the reactor, with a rate ranges from 30–33 sccm, to clean the substrates, and increase the reactivity of the precursor. TTIP has been heated at 80 °C, and then carried to the reactor by Ar gas till the pressure reached 15 Torr (2 kPa). Post deposition annealing has been carried out for 2 hours in air using a muffle furnace at temperatures ranging from 400 °C to 1100 °C.

### 2.2. Characterization of the films

Structural characterizations of the TiO<sub>2</sub> thin films have been carried out by X-ray diffraction (XRD).  $\theta - 2\theta$  scans have been recorded using Cu K $\alpha$  radiation in a Rigaku D-Max B diffractometer equipped with a graphite crystal monochromator.  $2\theta$  ranges from 20° to 70°. Raman spectroscopy has been recorded using Senterra Raman microscope, Bruker. A laser source of 532 nm wavelength has been used. Its power has been adjusted to be 10 mW. Thickness and morphology of the films have been measured by field emission scanning electron microscope, (FEI, Quanta 250 FEG). Optical transmission measurements have been carried out using a JASCO UV-350 spectrophotometer in the range from 300 to 1100 nm. Films have been annealed in air using a controlled temperature furnace. To measure the DC conductivity, two gold electrodes have been sputtered at the edges of the film to obtain ohmic contacts. Resistance has been measured by Keithly 612 electrometer as a function of temperature, and the corresponding DC conductivity has been calculated.

## 3. Results and discussions

### 3.1. Structure and morphology

XRD diffractograms for the as deposited sample, and those annealed up to 1100 °C are shown in Fig. 1. Using the powder diffraction files to identify the phase of the deposited and annealed films, it has been found that anatase is the only existing phase till 800 °C, and rutile appears at 900 °C.

The phase is mixed until 1100 °C. Something unexpected appears in these samples, which is the appearance of extra peaks in the samples annealed at 1000 °C and 1100 °C. To make sure, XRD investigation of quartz annealed at 1100 °C has been run. The obtained pattern does not show any peaks. The annealing process and the XRD measurements have been repeated without change in the results. In Fig. 1, the strongest peak (101) lies at  $2\theta$  equals 25.55°. Referring to powder diffraction file with reference code number 89-4921, one can find that the peak position of the main anatase peak is equal to that of the as deposited sample. This peak exists even if the sample annealed up to 1100 °C. At annealing temperature 900 °C the main rutile peak appears at  $2\theta$  equals 27.8°, which agrees with the standard peak found in powder diffraction file number 88-1172.

Two extra peaks appear in the sample annealed at 1000 °C. One of them is shown at 21.3° and the other at 27°. A third unidentified peak appears at 22.3° in the film annealed at 1100 °C. The appearance of unidentified peak close to 22° has been reported before for a sample deposited by sputtering.<sup>26</sup> But the appearance of another peak close to 27° has not been reported before. The crystallite size has been found to be 44 nm according to Debye–Scherrer equation.<sup>1</sup> This crystallite size is large compared to that of other nanoparticles prepared by the same technique.<sup>13</sup> Complete transformation to rutile depends on the anatase particle size, since small particles transform faster.<sup>13</sup> This may be the reason why rutile is not pure in this range of annealing. Such a delay in the rutile phase complete transformation has been attributed to the competition between

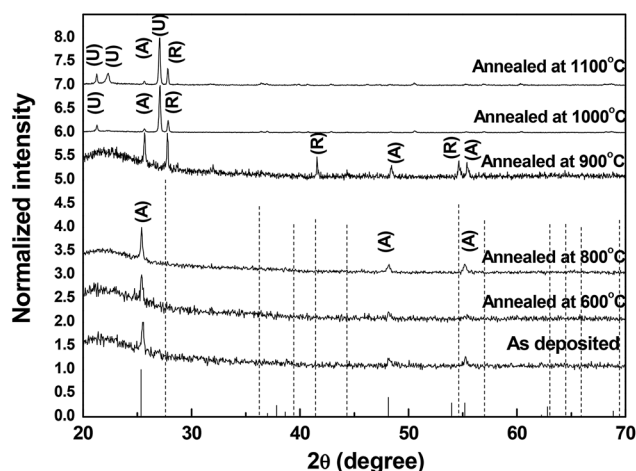


Fig. 1 X-ray diffraction patterns of the as-deposited TiO<sub>2</sub> film and films annealed up to 1100 °C.



two effects.<sup>27</sup> With the increase of annealing temperature, rutile phase nucleates, and grows also, the boundaries between crystallites at which anatase transforms to rutile decreases in volume. This reduction limits the nucleation, and growth of the rutile phase as seen in the XRD charts.

Since the anatase peaks diminish at high annealing temperatures, then the extra peaks may identify another form of rutile. We have to consider the relative intensity of the peak noticed at  $2\theta = 27^\circ$ . In other words, a new diffraction pattern of rutile is obtained in this study.

To assert the above conclusion, Raman spectra of the as deposited, and some of the annealed samples have been run, and presented in Fig. 2. Table 1 gives the peak positions of the Raman shifts.

Raman studies confirm XRD results. As shown in Fig. 2, the as deposited sample is a pure anatase while the annealed samples are mixed. The low frequency  $E_g$  peak appears in all the investigated samples. Also, the  $B_{1g}$ ,  $A_{1g}$ , and the higher frequency  $E_g$  modes of vibration characterizing the anatase phase appear in the as deposited sample.<sup>14,27,28</sup> Annealing at  $900^\circ\text{C}$  induces peaks mixing. A band is noticed at  $229.5\text{ cm}^{-1}$ , and it shows a blue shift with the increase of annealing temperature. This band is a higher order mode of vibration, and has been called a two phonon band.<sup>29,30</sup>

The film annealed at  $1100^\circ\text{C}$  demonstrates a low existence of the  $E_g$  anatase mode of vibration compared to the  $E_g$  and  $A_{1g}$  modes of the rutile phase.

From the spectrum depicted in Fig. 3, it can be noticed that there is no any other peak except a small hump at  $826\text{ cm}^{-1}$  which can be attributed to the  $B_{2g}$  mode of vibration of rutile.<sup>31</sup>

**Table 1** Modes of vibration of the as-deposited,  $900^\circ\text{C}$ , and  $1100^\circ\text{C}$  annealed samples

As-deposited	$900^\circ\text{C}$	$1100^\circ\text{C}$	Assignment
$143.5\text{ cm}^{-1}$	$141.5\text{ cm}^{-1}$	$142\text{ cm}^{-1}$	$E_g$ (anatase) low frequency
—	$229.5\text{ cm}^{-1}$	$235.5\text{ cm}^{-1}$	—
$397.5\text{ cm}^{-1}$	—	—	$B_{1g}$ (anatase)
—	$443.5\text{ cm}^{-1}$	$443.5\text{ cm}^{-1}$	$E_g$ (rutile)
$511.5\text{ cm}^{-1}$	—	—	$A_{1g}$ (anatase)
—	$609.5\text{ cm}^{-1}$	$607\text{ cm}^{-1}$	$A_{1g}$ (rutile)
$639\text{ cm}^{-1}$	—	—	$E_g$ (anatase) high frequency

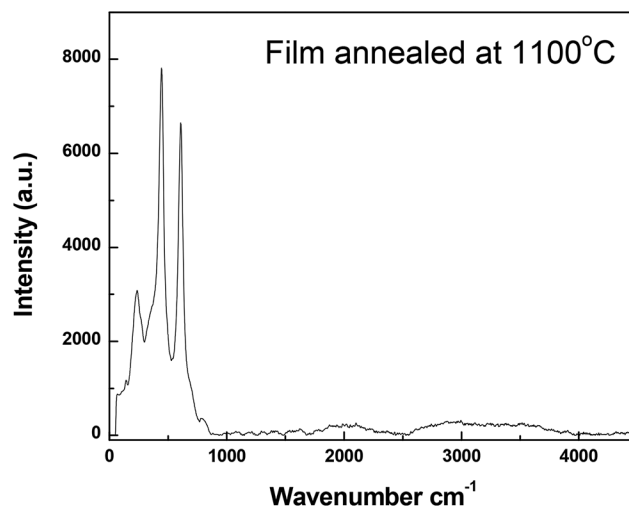


**Fig. 3** The complete spectrum of the film annealed at  $1100^\circ\text{C}$ .

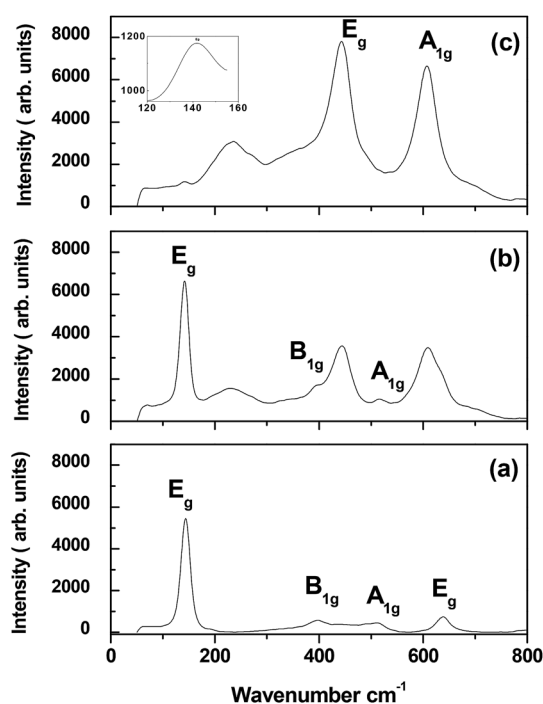


**Fig. 2** Raman spectra for samples (a) as deposited, (b) annealed at  $900^\circ\text{C}$ , and (c) annealed at  $1100^\circ\text{C}$ .

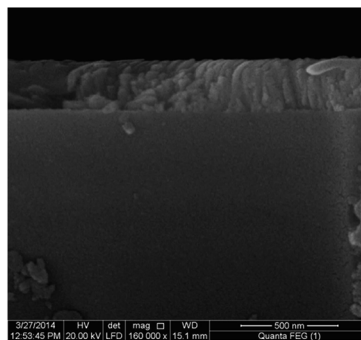
This spectrum confirms the above conclusion about the new diffraction pattern of rutile obtained in this study.

The thickness of the films has been determined by measuring the cross section of the annealed films. For example, the thicknesses of the  $600^\circ\text{C}$ , and  $900^\circ\text{C}$  annealed films have been found to be  $250 \pm 5\text{ nm}$  and  $260 \pm 10\text{ nm}$ , respectively.

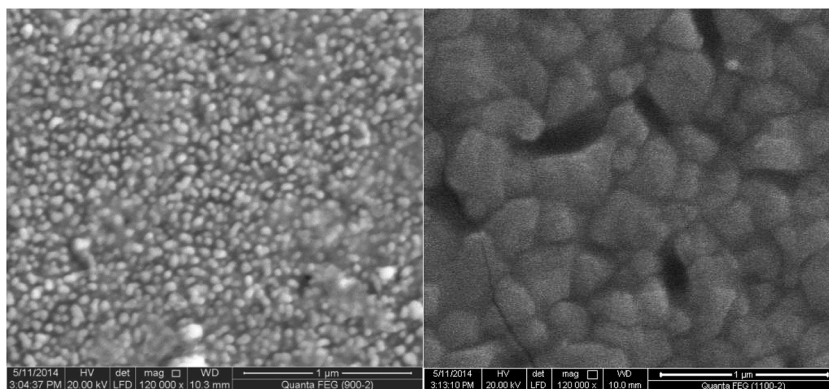
The morphology of the films has been monitored by FESEM studies as shown in Fig. 4. The as deposited film consists of clusters of small grains. Due to annealing the small grains coarsen, and fragment, and as a result the morphology has been changed to that shown in Fig. 4b. Such fragmentation has been reported before but for direct deposition with increasing the deposition temperature under the same pressure.<sup>10</sup> Further heating at  $900^\circ\text{C}$  shows something unusual for direct annealing. At this stage of phase transformation, the grain size decreases, it seems smaller compared to that of annealed at  $600^\circ\text{C}$ . Not only the size but also the shape of the grains changes due to heating. The grain size increases again when the sample annealed up to  $1100^\circ\text{C}$ .

The reported trend of the change in grain size with increasing the annealing temperature is the increase of particle size. This behavior has been elucidated by different tools in many reports. Table 2 shows the temperature ranges in which pure anatase transforms to rutile by sol-gel, spray pyrolysis and sputtering for some studies.



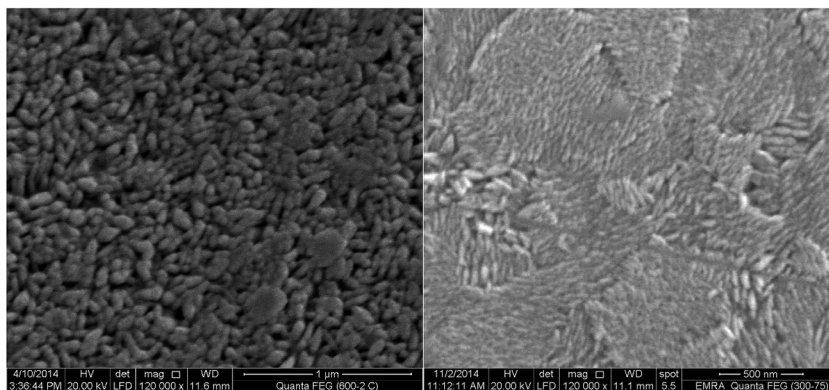


e) Cross section of the film annealed at 600°C.



c) Sample annealed at 900°C

d) Sample annealed at 1100°C.



a) As deposited sample at 300°C.

b) Sample annealed at 600°C.

Fig. 4 FESEM micrographs of as deposited film, films annealed at temperatures 600 °C, 900 °C, 1100 °C, and the cross section of the film annealed at 600 °C. (a) As deposited sample at 300 °C. (b) Sample annealed at 600 °C. (c) Sample annealed at 900 °C. (d) Sample annealed at 1100 °C. (e) Cross section of the film annealed at 600 °C.

Particle or grain size reduction before the crossover temperature, *i.e.* for pure anatase, has been reported for films and nanoparticles deposited by MOCVD at higher temperatures.<sup>9</sup> This decrease of particle size with the increase of deposition temperature under the same total pressure has been attributed to the increase of nucleation density which suppresses the calcination effects for powder nanoparticles. For thin films another explanation has been reported.<sup>10,23</sup> In this study, calcination effects only control the growth of anatase,

and the nucleation, and growth of rutile phases. Annealing at higher temperatures did not cause such particle size reduction for nanoparticle samples deposited by the same technique.<sup>13</sup> It is clear from the SEM images that calcination effects act traditionally until the appearance of the rutile phase. In other words, coarsening mechanism prevails. During phase transformation grain size reduction takes place. This event has not been reported for annealed films before. For example, Tu and Goto<sup>36</sup> reported an increase in the grain size with the increase in





Table 2 Phase transformation from anatase to rutile for some films

Deposition technique	Start of transformation	Complete phase transformation temperature	Used technique	Reference
MOCVD	700 °C	—	XRD, SEM	13
Normal sol-gel	650 °C, 450 °C sample, big crystallite size	850 °C, bad defined crystallite sizes	XRD, SEM	32
Ultrasound assisted sol-gel	650 °C, for 450 °C sample, small crystallite size, no agglomerations	750 °C, 850 °C sample lesser, agglomerations and well defined crystallite sizes	XRD, SEM	32
Sol-gel	800 °C	900 °C	XRD, SEM	33
Spray pyrolysis	800 °C	1000 °C	XRD, AFM, SEM 50 nm	14
Sputtering	700 °C	900 °C	XRD, AFM	34
Sputtering	650 °C	750 °C	XRD (23.3 nm), SEM	35

annealing temperature without any reduction at the crossover temperature. Won *et al.*<sup>37</sup> deposited TiO<sub>2</sub> thin films at the same temperature by the same technique, and precursor with slight deposition condition differences. They did not notice the reported reduction in grain size due to annealing. This may be because the percent of the rutile phase in their mixed phase sample was small as seen in their XRD pattern. If we calculate the weight percent of the rutile at this temperature using the formula:<sup>21</sup>

$$w_R = I_R/I_o = I_R/(0.994I_A + I_R) \quad (2)$$

where  $w_R$  is the weight percent of the rutile phase,  $I_R$  is the intensity of the (110) rutile peak,  $I_A$  is the intensity of the (101) anatase peak, and  $I_o$  is the total intensity of the two mentioned peaks, it will equal 55%. According to the phase transformation model proposed by Zhang *et al.*,<sup>38</sup> and confirmed by Li *et al.*<sup>13</sup> for powder nanoparticles which can be also applied for thin films, rutile nucleation is controlled by surface nucleation (surface nucleation > interface nucleation > bulk nucleation). Consequently, rutile grows at the expense of anatase at the surfaces and interfaces. Phase transformation in TiO<sub>2</sub> is a reconstructive process.<sup>39</sup> So, it involves breaking of existing bonds and the formation of a new set. Moreover, lattice contraction cannot be ignored. Lattice contraction with the increase of crystallite size of anatase during phase transformation has been attributed to added stresses because of crystallites merging and/or rutile phase precipitation.<sup>13</sup> Lattice expansion with the decrease of grain size has been ascribed to electrostatic relaxation.<sup>40</sup> Lattice contraction in this study results from anatase to rutile transformation since the ratio of volumes between anatase and rutile unit cells is 2.2. Both crystallite size, and grain size is a number of unit cells. Since the weight percent of the two phases are nearly equal, the part which has been transformed to rutile may suffer from grain reduction. So, anatase consumption, rutile nucleation, and/or surface reconstruction may drive the observed grain size reduction during anatase to rutile transformation.

### 3.2. Optical properties

UV-Vis spectrophotometric measurements have been carried out for the as deposited sample and those annealed at 600 °C, and 900 °C and presented in Fig. 5.

Absorption coefficient  $\alpha$  can be calculated from the relation:

$$T = (1 - R)^2 \exp(-\alpha d) / 1 - R^2 \exp(-\alpha d) \quad (3)$$

where  $R$ , and  $T$  are the spectral reflectance, and transmittance, and  $d$  is the film thickness. At normal incidence this equation can be approximated to:<sup>41,42</sup>

$$\alpha = (1/d) \ln(1/T) \quad (4)$$

The energy gap for indirect band gap transition can be calculated from:<sup>42</sup>

$$\sqrt{\alpha h\nu} = (E_g - h\nu + E_{ph}) + (E_g - h\nu - E_{ph}) \quad (5)$$

The obtained optical energy gap values are 3.28 eV, 3.2 eV and 3.14 eV for deposition temperature 300 °C and the annealing temperatures 600 °C, and 900 °C, respectively. It is clearly seen that the band gap decreases with the increase of annealing temperature. This behavior is the expected according to that published in literature (Fig. 6).<sup>14,37</sup>

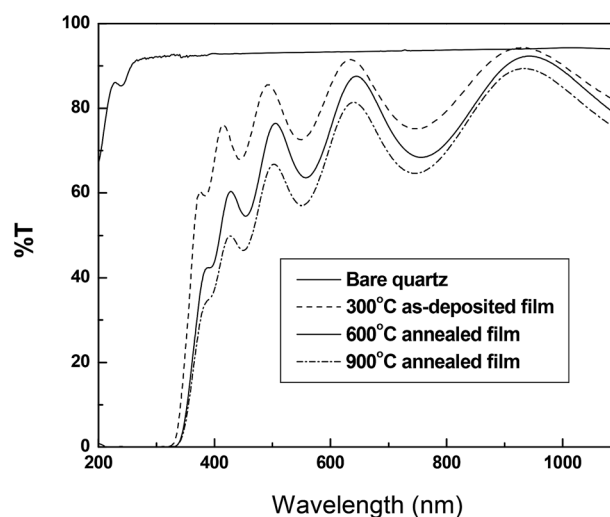


Fig. 5 Transmittance spectra as a function of wavelength for bare quartz substrate, as-deposited film and films annealed at 600 °C, and 900 °C.



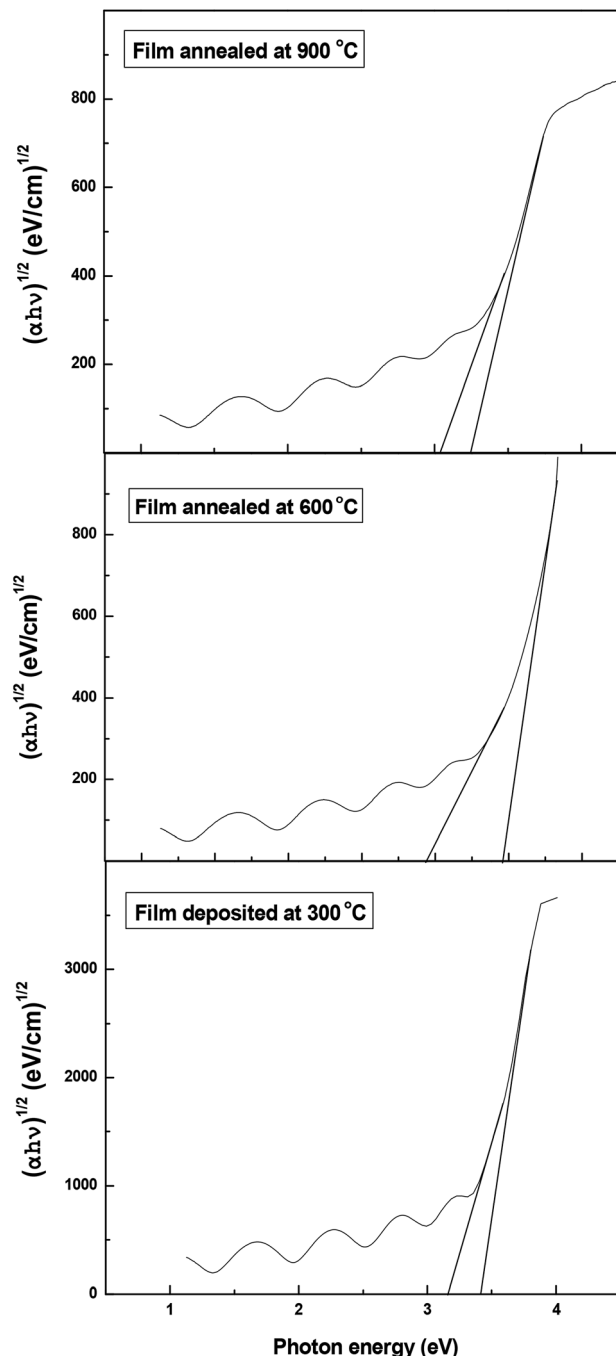


Fig. 6  $\sqrt{\alpha h\nu}$  versus photon energy for as deposited sample and those annealed at 600 °C, and 900 °C.

### 3.3. Electrical properties

DC conductivity measurements have been run for samples annealed at 600 °C, and 900 °C. The natural logarithm as a function of the reciprocal of absolute temperature is depicted in Fig. 7.

It shows that the obtained curve can be divided into three regions. The results do not show smooth curve because of switching between the electrometer ranges. The first part is nearly temperature independent in the range from room temperature to about 130 °C (273–403 K). Temperature

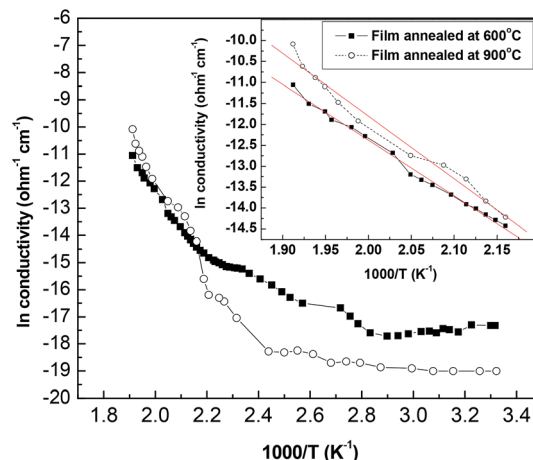


Fig. 7  $\ln \sigma$  as a function of  $1000/T$  for samples annealed at 600 °C, and 900 °C.

independent attitude has been found in the range from 13–230 K for anatase by Mardare and Rusu.<sup>43</sup> They attributed the conduction behavior to nonstoichiometry. Anatase sample reduced at 450 °C under vacuum show an insulator to metal transition in the temperature range from 80–280 K.<sup>28</sup> Also, highly reduced rutile showed activation energy equals 0.06 eV in the same temperature range.<sup>28</sup> At higher temperature in the range from room temperature to 345 K Akl *et al.* obtained an activation energy equals 0.03 eV.<sup>44</sup>

An intermediate increase in conductivity takes place in the temperature range from 130 °C to 190 °C (403–463 K). Akl *et al.* noticed a similar trend with activation energy equals 0.17 eV.<sup>44</sup> Deviation from linearity in the curve relating the logarithm of resistivity, and the reciprocal of absolute temperature in the range from 409–463 K has been found by Deshmukh *et al.*<sup>41</sup> In the temperature range from 360–500 K Mardare, and Rusu proved linearity with activation energy equals 0.72 eV.<sup>43</sup>

High activation energy conductivity prevails in the temperature range from 190 °C to 250 °C (463–523 K). In the later temperature range the activation energy has been calculated from the equation:<sup>43</sup>

$$\ln \sigma = \ln \sigma_0 - E_a/kT \quad (6)$$

where  $\sigma$  is the conductivity,  $\sigma_0$  is a constant,  $E_a$  is the activation energy,  $k$  is Boltzmann's constant, and  $T$  is the absolute temperature. The activation energy values are 1.15 eV and 1.29 eV for the 600 °C and 900 °C films, successively.

Activation energy depends on the type of the substrate, grain size, and phase.<sup>45–47</sup> Also, the activation energy value depends on the temperature range for which it is calculated.<sup>44</sup> Oxygen partial pressure plays a critical role in transport properties of metal oxides.<sup>28,44</sup>

The three regions obtained in this study resemble those obtained by Akl *et al.* for samples deposited by reactive RF sputtering but with different values of conductivities, and activation energies.<sup>44</sup> This can be attributed to the deposition conditions, and post deposition treatment in the two cases.



Deposition of the samples on this study involves reaction in the presence of oxygen at 300 °C, and leaving the samples to cool down to room temperature in the presence of oxygen. Moreover, annealing in this study has been carried out in air, while in their study it has been carried out under vacuum at temperatures 400 °C, 450 °C and 500 °C, respectively. Such annealing reduces the deposited material which causes semiconductor to metal transition for anatase annealed at 450 °C.<sup>28</sup> Oxygen vacancies create donor energy states below the conduction band. Depending on the concentration of these created levels Fermi level moves toward the conduction band. So, the activation energy will inversely proportional to the concentration of oxygen vacancies.

It can be concluded that annealing in air and its influences on the structural and morphological properties of TiO<sub>2</sub> thin films did not make significant changes on the electrical conductivity, and activation energy of the obtained films if experimental errors have been taken into consideration.<sup>43,48</sup>

## 4. Conclusion

TiO<sub>2</sub> thin films have been deposited by MOCVD at 300 °C, and subsequently annealed till 1100 °C. Films deposited, and annealed till 800 °C are pure anatase. Rutile phase starts to appear at 900 °C. Extra unidentified peaks have been detected in the films annealed at 1000 °C, and 1100 °C. SEM micrographs revealed a regular calcination effects but anomalous reduction in the grain size synchronizes the detection of the rutile phase. A new diffraction pattern of rutile has been noticed in this study according to the analysis of the XRD, and Raman data. Optical properties show a regular trend while electrical conductivity suggested three different activation energies.

## Acknowledgements

The author would like to thank the nano-materials and nano-technology lab team at Beni – Suef University for their help. Also, I would like to thank Prof. Kamal Abdel-Hady and his group in El-Minia University for their help regarding DC conductivity measurements.

## References

- 1 Z. S. Khalifa, *Sol. Energy Mater. Sol. Cells*, 2014, **124**, 186.
- 2 C. Natarajan, N. Fukunaga and G. Nogami, *Thin Solid Films*, 1998, **322**, 6.
- 3 F. Men, X. Song and Z. Sun, *Vacuum*, 2009, **83**, 1147.
- 4 M. Grätzel, *Nature*, 2000, **414**, 344.
- 5 B. O'Regan and M. Grätzel, *Nature*, 1991, **353**, 737.
- 6 H. Kim, M. Hong, H. Jang, S. Yoon and H. Park, *Thin Solid Films*, 2013, **529**, 89.
- 7 B. Zachau-Christiansen, K. West, T. Jacobsen and S. Atlung, *Solid State Ionics*, 1988, **28–30**, 1176.
- 8 J. M. Wu, H. C. Shih and W. T. Wu, *Chem. Phys. Lett.*, 2005, **413**, 490.
- 9 W. Li, S. Ismat Shah, M. Sung and C.-P. Huang, *J. Vac. Sci. Technol., B*, 2002, **20**, 2303.
- 10 C. J. Taylor, D. C. Gilmer, D. G. Colombo, G. D. Wilk, S. A. Campbell, J. Roberts and W. L. Gladfelter, *J. Am. Chem. Soc.*, 1999, **121**, 5220.
- 11 T. L. Hill, *Thermodynamics of Small Systems*, W. A. Benjamin, New York, NY, 1963, vol. I.
- 12 T. L. Hill, *Thermodynamics of Small Systems*, W. A. Benjamin, New York, NY, 1964, vol. II.
- 13 W. Li, C. Ni, H. Lin, C. P. Huang and S. Ismat Shah, *J. Appl. Phys.*, 2004, **96**, 6663.
- 14 A. Nakaruk, D. Ragazzon and C. C. Sorrell, *Thin Solid Films*, 2010, **518**, 3735.
- 15 M. Matsui and M. Akaogi, *Mol. Simul.*, 1991, **6**, 239.
- 16 S. Smith, R. Stevens, S. Liu, G. Li, A. Navrotsky, J. Boerio-Goates and F. Woodfield, *Am. Mineral.*, 2009, **94**, 239.
- 17 P. M. Oliver, G. W. Watson, T. E. Kelsey and C. S. Parker, *J. Mater. Chem.*, 1997, **7**, 563.
- 18 M. Lazzeri, A. Vittadini and A. Selloni, *Phys. Rev. B: Condens. Matter Mater. Phys.*, 2001, **63**, 15540.
- 19 M. Lazzeri, A. Vittadini and A. Selloni, *Phys. Rev. B: Condens. Matter Mater. Phys.*, 2002, **65**, 11990.
- 20 U. Diebold, N. Ruzicky, G. S. Herman and A. Selloni, *Catal. Today*, 2003, **85**, 93.
- 21 A. A. Gribb and J. F. Banfield, *Am. Mineral.*, 1997, **82**, 717.
- 22 H. Zhang and J. F. Banfield, *J. Mater. Chem.*, 1998, **8**, 2073.
- 23 Z. S. Khalifa, H. Lin and S. Ismat Shah, *Thin Solid Films*, 2010, **518**, 5457.
- 24 Y. Sun, A. Li, M. Qi, L. Zhang and X. Yao, *Mater. Sci. Eng. B*, 2001, **86**, 185.
- 25 B. Roy, G. Zhang and J. Cho, *J. Am. Ceram. Soc.*, 2012, **95**, 676.
- 26 D. Yoo, I. Kim, S. Kim, C. Hahn, C. Lee and S. Cho, *Appl. Surf. Sci.*, 2007, **253**, 3888.
- 27 H. Rath, P. Dash, T. Som, P. Satyam, U. Singh, P. Kulriya, D. Kanjilal, D. Avasthi and N. Mishra, *J. Appl. Phys.*, 2009, **105**, 074311.
- 28 H. Tang, K. Prasad, R. Sanjinbs, P. Schmid and F. Levy, *J. Appl. Phys.*, 1994, **75**, 2042.
- 29 C. Rosário, M. Grac, M. A. Valente, L. Costa, J. Rodrigues, T. Monteiro, E. Alves and N. Sobolev, *Phys. Status Solidi B*, 2013, **250**, 843.
- 30 B. Santara, P. Giri, K. Imakita and M. Fujii, *J. Phys. D: Appl. Phys.*, 2014, **47**, 215302.
- 31 C. Chen, Y. Chen, A. Korotcov, Y. Huang, D. Tsai and K. Tiong, *Nanotechnology*, 2008, **19**, 075611.
- 32 K. Prasad, D. V. Pinjari, A. B. Pandit and S. T. Mhaske, *Ultrason. Sonochem.*, 2010, **409**, 17.
- 33 A. Nakaruk, C. Y. Lin, D. S. Perera and C. C. Sorrell, *Sol-Gel Sci. Technol.*, 2010, **55**, 328.
- 34 Y. Hou, D. Zhuang, G. Zhang, M. Zhao and M. Wu, *Appl. Surf. Sci.*, 2003, **218**, 98.
- 35 B. Sarma, A. Pal, H. Bailung and J. Chutia, *J. Alloys Compd.*, 2013, **577**, 261.
- 36 R. Tu and T. Goto, *Mater. Trans.*, 2008, **49**, 2040.
- 37 D. Won, C. Wang, H. Jang and D. Choi, *Appl. Phys. A*, 2001, **73**, 595.
- 38 H. Zhang and J. Banfield, *Am. Mineral.*, 1999, **84**, 528.
- 39 G. Herman and Y. Gao, *Thin Solid Films*, 2001, **397**, 157.



- 40 M. Ahmad and S. Bhattacharya, *Appl. Phys. Lett.*, 2009, **95**, 191906.
- 41 H. P. Deshmukh, P. S. Shinde and P. S. Patil, *Mater. Sci. Eng. B*, 2006, **130**, 220.
- 42 A. Kumar, P. Singh, N. Kulkarni and D. Kaur, *Thin Solid Films*, 2008, **516**, 912.
- 43 D. Mardare and G. Rusu, *Mater. Sci. Eng. B*, 2000, **75**, 68.
- 44 A. Akl, H. Kamal and K. Abdel-Hady, *Appl. Surf. Sci.*, 2006, **252**, 8651.
- 45 B. Huber, H. Gnaser and C. Ziegler, *Surf. Sci.*, 2004, **566–568**, 419.
- 46 B. Huber, A. Brodyanski, M. Scheib, A. Orendorz, C. Ziegler and H. Gnaser, *Thin Solid Films*, 2005, **472**, 114.
- 47 I. Oja, A. Mere, M. Krunk, R. Nisumaa, C.-H. Solterbeck and M. Es-Souni, *Thin Solid Films*, 2006, **515**, 674.
- 48 M. Sekhar, P. Kondaiah, S. Chandra, G. Rao and S. Uthanna, *Appl. Surf. Sci.*, 2011, **258**, 1796.

